Engineering Structures 30 (2008) 3399–3411

Contents lists available at ScienceDirect

Engineering Structures

journal homepage: www.elsevier.com/locate/engstruct

Analytical prediction of the seismic behaviour of superelastic shape memory alloy reinforced concrete elements

M.S. Alam, M.A. Youssef, M. Nehdi *

Department of Civil and Environmental Engineering, The University of Western Ontario, London, Ontario, Canada, N6A 5B9

ARTICLE INFO

Article history:
Received 11 November 2007
Received in revised form
18 May 2008
Accepted 19 May 2008
Available online 27 June 2008

Keywords:
Shape memory alloy
Superelasticity
Beam–column joint
Plastic hinge length
Crack
Moment–rotation
Load–displacement

ABSTRACT

Superelastic shape memory alloys (SMAs) are unique materials that have the ability to undergo large deformations, but can return to their undeformed shape by the removal of stress. If such materials can be used as reinforcement in plastic hinge regions of beam–column elements, they will not only experience large inelastic deformations during strong earthquakes, but can potentially recover their original shape. This behaviour will allow mitigating the problem of permanent deformation. Hence, this study aims at establishing guidelines for predicting the seismic behaviour of concrete beam–column elements reinforced with superelastic SMAs. The paper identifies the disparities in moment–curvature relationship between SMA and steel reinforced sections. Then it examines the applicability of existing methods developed for steel reinforced concrete (RC) members to predict the length of the plastic hinge, crack width, crack spacing, and bond-slip relationship for superelastic SMA RC elements. Existing superelastic SMA models are discussed and the application of one of the models in a finite element (FE) program is presented. This FE program is used to simulate the behaviour of an SMA RC column and a beam–column joint. The predicted load–displacement, moment–rotation relationships and energy dissipation capacities have been found to be in good agreement with experimental results.

1. Introduction

Buildings and bridges in high seismic regions are prone to severe damage and collapse during earthquakes due to large lateral deformations. In particular, beam–column elements in reinforced concrete (RC) structures are extremely vulnerable and are considered the weakest link in such a structural system [1]. Current seismic design codes emphasize earthquake resistant structures to be sufficiently ductile by proper reinforcement detailing at critical regions in order to ensure elastic behaviour under moderate earthquakes. However, it is difficult and costly to build structures that can perform elastically under strong ground motion. In conventional seismic design of RC structures, reinforcing bars are expected to yield in order to dissipate energy while undergoing permanent deformations of post-yield steel reinforcing bars and damage of unconfined concrete. Consequently, during large-scale earthquake events, severe damage of infrastructure occurs resulting in the collapse of buildings, closing of bridges, unattainable post-disaster rescue operations, and overall substantial economic losses. These can generally be avoided if structures were serviceable after such earthquakes.

Superelastic (SE) SMA is a special material that can undergo large inelastic deformations and recover its original shape by stress removal, thus mitigating the problem of permanent deformation. Because of its unique characteristics, SMAs have gained increased usage in structural applications [2] for instance, as column anchorage [3], frame bracing [4], concrete prestressing [5], damping device [6,7], and bridge restrainers [8]. Ocel et al. [9] used SMAs in steel beam–column connections, which displayed repeatable and stable hysteretic behavior. Auricchio et al. [10] and Zhu and Zhang [11] conducted numerical simulations and compared the seismic responses of steel frame buildings equipped with traditional steel bracings and SE SMA bracings. Their results showed that buildings with SMA bracings performed better than steel braced buildings in terms of inter-storey and residual drift. Krstulovic-Opara et al. [12] performed a numerical investigation on the use of high-performance concrete reinforced with SMA fibres and its effect on the structural response of a SMA-HPFRC frame structure. Saiidi et al. [13] investigated the effectiveness of SE SMA RC beams in reducing permanent deformation where SMA was used as tensile reinforcement only at the critical region of the beam. Recent tests conducted by Saiidi and Wang [14] and Youssef et al. [15] showed that SE SMA RC elements are capable of dissipating significant amounts of energy with negligible residual deformation and rotation during earthquakes. This extraordinary characteristic of SE SMA-RC beam–column elements can be of great benefit in high seismic areas as RC members will remain functional even after a strong earthquake. SMAs' high strength, large energy hysteretic behaviour, full recovery of strains up to

* Corresponding author. Tel.: +1 519 661 2111x88308; fax: +1 519 661 3779.
E-mail address: mnehdi@eng.uwo.ca (M. Nehdi).

0141-0296/$ – see front matter © 2008 Elsevier Ltd. All rights reserved.
doi:10.1016/j.engstruct.2008.05.025

List of Notations

f_y	Yield stress of rebar; SMA's yield is being used to refer to the initiation of phase transformation, i.e. Austenite to martensite starting stress of SMA (Fig. 1(b))
f_{P1}	Maximum stress of SMA up to its superelastic strain range (Fig. 1(b))
f_{T1}	First stage of unloading stress of SMA (Fig. 1(b))
f_{T2}	Second stage of unloading stress of SMA (Fig. 1(b))
ε_l	Superelastic plateau strain length of SMA (Fig. 1(b))
E_s	Modulus of elasticity of SMA in martensite state
E_a	Modulus of elasticity of SMA in austenite state
α	The ratio of f_y under tension and compression
A_f	Austenite finish temperature
θ_e	Elastic rotation
θ_p	Plastic rotation
L	Length of the member
L_p	Plastic hinge length
ϕ_y	Curvature at which rebar yields
ϕ_u	Maximum curvature in the inelastic range
Δ_y	Displacement at which rebar yields
Δ_u	Maximum displacement in the inelastic range
d	Effective depth of the member
d_b	Bar diameter
ε_s	Strain in the rebar
C	Concrete clear cover
S	Maximum spacing between longitudinal rebars
S_{ave}	Average spacing between longitudinal rebars
A_{ceff}	Effective tensile area of concrete surrounding the tension rebars and having the same centroid as that of the rebars
A_{s1}	Area of each rebar
f'_c	Concrete compressive strength
w_m	Mean crack width
$w_{\max}$	Maximum crack width
S_m	Crack spacing
h_1	Distance from the centroid of the tension rebar to the neutral axis
h_2	Distance from the extreme tension fiber to the neutral axis
n	Number of rebar in the tension zone
ε_1	Maximum tensile strain in the effective zone
ε_2	Minimum tensile strain in the effective zone
A_s	Area of rebar in the tensile zone
f_s	Stress in the reinforcement at specified loads calculated using elastic cracked section theory
d_c	Distance from the extreme tension fiber to the center of the rebar located closest to it
k	A coefficient which is equal to 11×10^{-6} for conventional RC members, found as $40.9 \times 10^{-6} \pm 9.5 \times 10^{-6}$ for FRP RC members
ρ	Reinforcement ratio
E_s	Modulus of elasticity of rebar
k_1	A coefficient having a value of 1.6 for plain bars and 0.8 for deformed bars
k_2	A coefficient having a value of 0.5 for members subjected to bending and 1.0 for members subjected to tension
s_{st}	Axial elongation of steel
s_{SMA}	Axial elongation of SMA
s_e	Extensometer reading from the pullout test
s	Bar slip at the joint
T	Bar force from the pullout test
P	Force applied at the beam tip of the beam–column joint
h	Beam depth
d'	Distance from the centre of the top bar to the top beam face

8%, high resistance to corrosion and fatigue make them strong contenders for use in earthquake resistant structures [16]. In particular, Ni–Ti alloy has been found to be the most promising SMA for seismic applications.

This paper examines the fundamental characteristics of SE SMA and its modelling technique. It also aims at defining methods to predict the behaviour of superelastic SMA RC beam–column elements in terms of its moment–curvature relationship, plastic hinge length, crack width, crack spacing, and bond-slip relationship. Nonlinear FE analysis has been implemented in this study to predict the load–displacement relationship and energy dissipation capacity of superelastic SMA RC beam–column elements. These predictions are compared with experimental results.

2. Research significance

The seismic design of structures has evolved towards a performance-based approach in which there is need for new structural members and systems that possess enhanced deformation capacity and ductility, higher damage tolerance, decreased residual crack size, and recovered or reduced permanent deformations. The use of superelastic SMA as reinforcement instead of steel in the hinge locations of beams and columns has not only proved to dissipate adequate seismic energy, but could also restore the original shape of such members after seismic actions. Such SMA reinforced beam–column elements could allow structural engineers to design RC connections exhibiting little damage and mitigating post earthquake joint repairs. SMA has a relatively lower modulus of elasticity and smaller hysteretic loop compared to that of steel. Therefore, using SMA as reinforcement in RC sections may result in significant changes in the behaviour of RC structures, thus having practical importance in their design. This paper discusses critical and essential design features of SMA RC structures from the analytical point of view. It provides numerical tools and guidelines that should prove to be essential for designers in the near future.

3. Superelastic shape memory alloys

Superelasticity is a distinct property that makes SMA a smart material. A SE SMA can restore its initial shape spontaneously even from its inelastic range upon unloading. Among various composites, Ni–Ti has been found to be the most appropriate SMA for structural applications because of its large recoverable strain, superelasticity and exceptionally good resistance to corrosion. In this paper, unless otherwise stated, SMAs are mainly referred to Ni–Ti SMA (commonly known as Nitinol).

A SMA exhibits superelasticity as long as it is in the austenite state. When an austenite SMA is loaded and unloaded, six distinctive characteristics can be recognized in the stress strain diagram (Fig. 1(a)): (a) elastic response of austenite at low strains ($<$1%) as denoted by BC, (b) stress-induced transformation from austenite to martensite with a long and constant stress plateau at intermediate and large strains as indicated by CD, (c) elastic response in the stress-induced martensite state at large strains represented by DE, (d) elastic recovery of strain upon stress removal as shown by EF, (e) instinctive recovery of strain at almost a constant stress path because of the reverse transformation to austenite due to the instability of martensite as depicted by FG, and finally (f) elastic recovery in the austenite phase as indicated by GB [16]. This exceptional ability of SMA to recover substantial inelastic deformation upon unloading yields a characteristic hysteresis loop, which is known as superelasticity. SMA with superelasticity has an advantage over other common metals/alloys in the sense that besides dissipating a considerable amount of energy under repeated load cycles, it has a negligible residual strain.

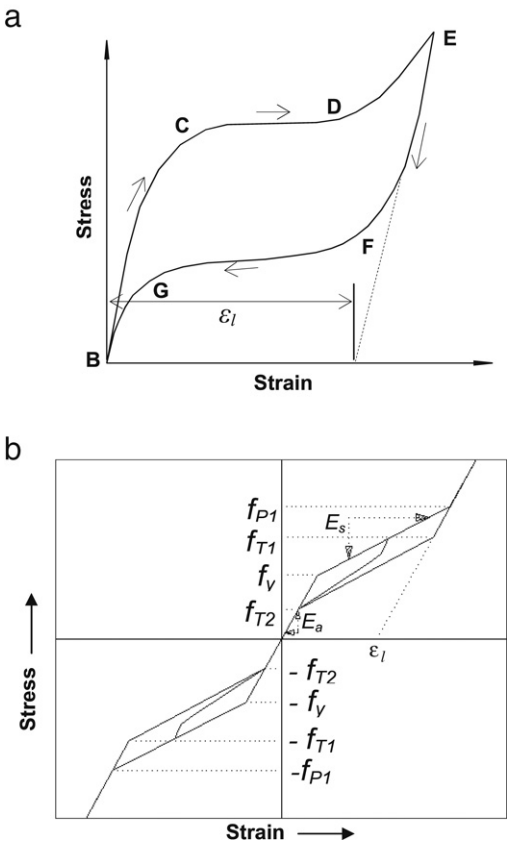

Fig. 1. (a) Typical axial stress–strain diagram of superelastic SMA, (b) 1D-superelastic model of SMA incorporated in FE Pacakges (reprinted from Auricchio et al. [24] with permission).

3.1. Modeling SMA

Since most civil engineering applications of SMA are related to the use of bars and wires, one-dimensional phenomenological models are often considered suitable. Several researchers have proposed uniaxial phenomenological models for SMA [17–20]. The superelastic behavior of SMA has been incorporated in a number of finite element packages, e.g. ANSYS 10.0 [21], ABAQUS 6.4 [22] and Seismostruct 4.0.2 [23] where the material models have been defined using the models of Auricchio et al. [24], Auricchio and Taylor [25], and Auricchio and Sacco [26], respectively. Fig. 1(b) shows the 1D-superelastic model used in ANSYS 10.0 [21] where SMA has been subjected to multiple stress cycles at a constant temperature and undergoes stress induced austenite-martensite transformation. The parameters used to define the material model (Fig. 1) are yield stress, f_y (point C); maximum stress up to the superelastic strain range, f_{P1} (point E); first stage of unloading stress, f_{T1} (point F); second stage of unloading stress, f_{T2} (point G); superelastic plateau strain length, ε_l; moduli of elasticity, E_s and E_a; and the ratio of f_y under tension and compression, α. Although a SMA does not have a yielding process, yield is being used to refer to the initiation of phase transformation of SMA. Fig. 2 shows stress–strain curves of the SMA model [24] with a complete transformation path followed by (a) cycles with partial loading (PL) and partial unloading (PU), (b) cycles with PL and complete unloading (CU), and (c) cycles with complete loading (CL) and PU, respectively. Here, PL and PU refer to incomplete stress induced phase transformation, whereas CL and CU refer to complete stress induced transformation in the loading-unloading process. Fig. 2 highlights the stress–strain behavior of SE SMA under cyclic axial loading of varying amplitudes.

4. Experimental study on SMA RC elements

This section briefly describes the available experimental studies conducted on SMA RC beam–column elements under seismic loading.

4.1. SMA RC beam–column joint

Two large-scale beam–column joints were tested under reversed cyclic loading by Youssef et al. [15]. The first joint was reinforced with regular steel rebars, while the other was reinforced with SMA at the plastic hinge region of the beam, along with regular steel in the remaining portion of the joint (specimen JBC-2). Hot-rolled Ni–Ti alloy (55.0% nickel and 45.0% titanium by weight) rebar was used as reinforcement in the JBC-2 specimen. Its austenite finish temperature, A_f, defining the complete transformation from martensite to austenite, ranges from −15 to −10 °C. Both joints were designed according to Canadian standards [27]. The detailed design of joints JBC-1 and JBC-2 is given in Fig. 3(a). In the case of JBC-2, single barrel screw lock couplers [28] were used for connecting steel and SMA rebars. The couplers used are mechanical connectors consisting of smooth shaped steel sleeves with converging sides. Each end of the reinforcing bars is inserted into one of the coupler ends until it reaches the middle pin (center stop). Both rebars meet head to head separated by a pin at the middle. Screws with smooth ends are used to hold the rebars, which are tightened until their heads are sheared off indicating that the required torque is reached. Fig. 3(b) and (c) illustrate the splice details and couplers used in the reinforcement caging of JBC-2, respectively. The material properties for both specimens are presented in Table 1. Some experimental results of both specimens in terms of yield and ultimate values of curvatures and beam-tip displacements, plastic hinges, crack width and crack spacing are presented in Tables 2 and 3.

4.2. SMA RC column

Two quarter-scale spiral RC columns representing RC bridge piers were designed, constructed and tested using a shake table by Saiidi and Wang [14]. Fig. 4 shows the reinforcement detailing of the bridge pier (specimen SMAC-1) where SMA rebars are placed

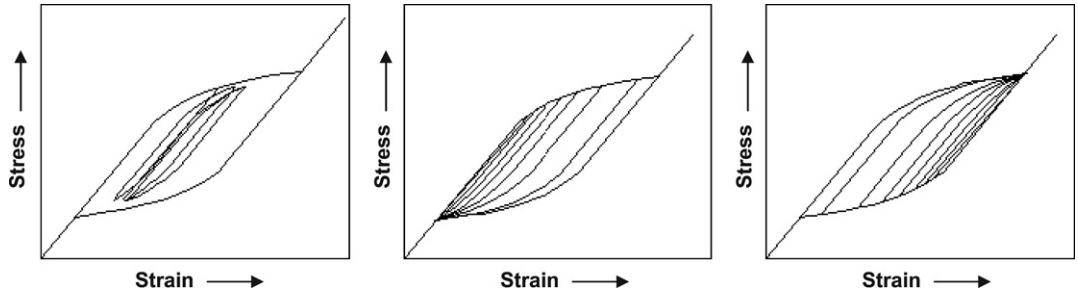

Fig. 2. 1D-Superelastic model of SMA at constant temperature where the stress–strain curves are drawn after a complete transformation path followed by (a) PL and PU, (b) PL and CU, and (c) CL and PU (reprinted from Auricchio et al. [24] with permission).

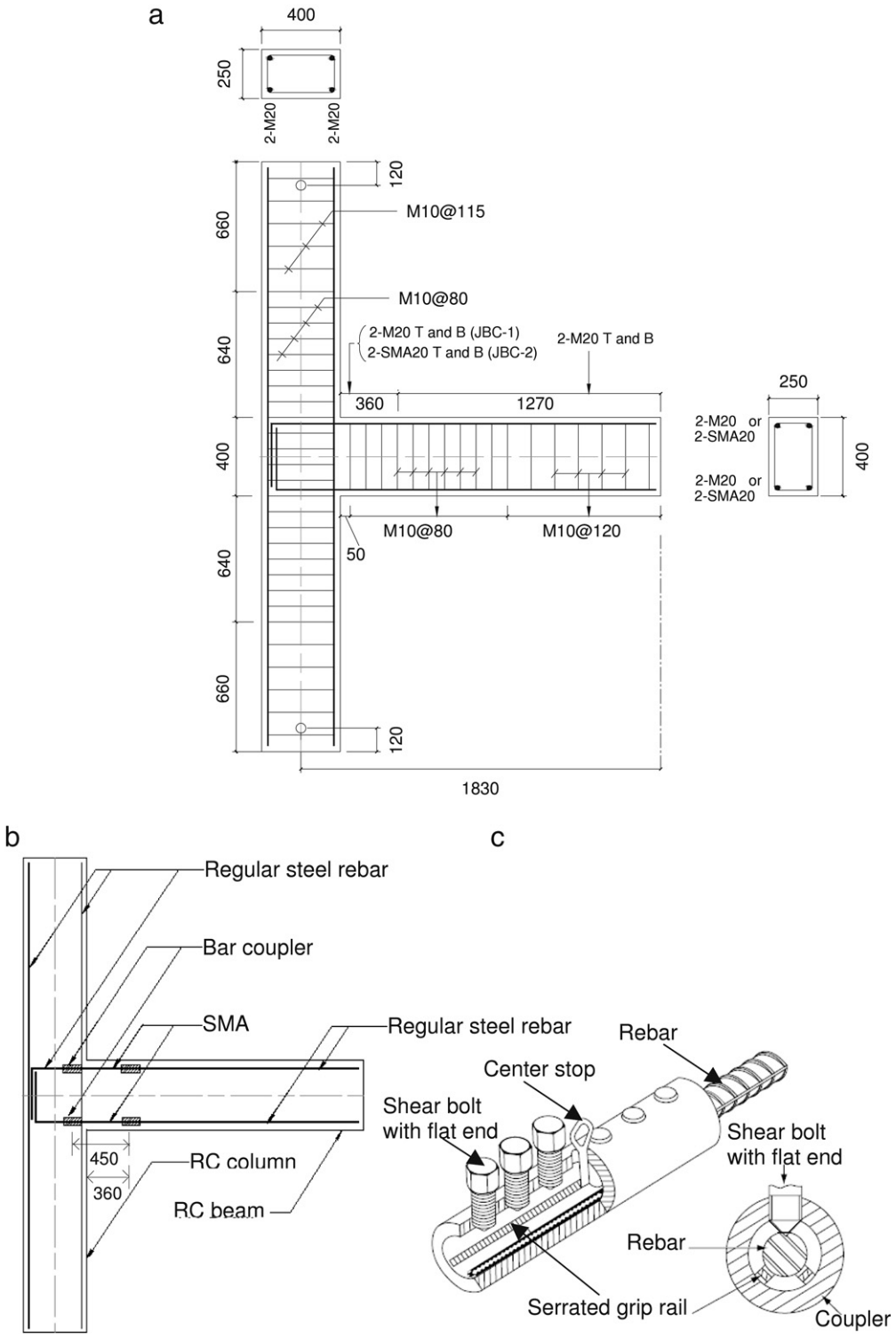

Fig. 3. (a) Reinforcement details of specimens JBC-1 and JBC-2, (b) Splice details of specimen JBC-2, (c) single barrel screw-lock coupler for connecting SMA rebar with regular steel rebar (all dimensions in mm).

at the plastic hinge region and connected to the steel rebars with threaded mechanical couplers. Ni–Ti alloy (55.9% nickel and 44.1% titanium by weight) with austenite finish temperature, A_f of approximately 0 °C was used as reinforcement. The mechanical properties of the materials used are presented in Table 1. The yield and ultimate values of curvature and top-displacement, and the length of the plastic hinge of the column are presented in Table 2. Saiidi and Wang [14] observed that SMA-RC columns were superior to conventional steel-RC columns in limiting relative column top displacement and overall residual displacements; they withstood larger earthquake amplitudes compared to that for conventional columns.

5. Analytical prediction

This section deals with the analytical prediction of moment–curvature, plastic hinge length, crack width and crack spacing of

Table 1
Material properties for specimens JBC-1, JBC-2 and SMAC-1

Material	Property	JBC-1	JBC-2	SMAC-1
Concrete	Compressive strength (MPa)	53.5	53.7	43.8
	Strain at peak stress (%)	0.2	0.2	0.2
	Tensile strength (MPa)	3.5	2.8	4.0
Longitudinal steel (JBC-1 & 2: Ø19.5 mm, SMAC-1: Ø15.9 mm)	Yield strength (MPa)	520	450	439
	Ultimate strength (MPa)	630	650	708
	Young's modulus (GPa)	198	193	200
Transverse steel (JBC-1 & 2: Ø11.3 mm, SMAC-1: Ø4.9 mm)	Yield strength (MPa)	422	422	469
	Ultimate strength (MPa)	682	682	540
SE SMA (JBC-1 & 2: Ø20.6 mm, SMAC-1: Ø12.7 mm)	Modulus of elasticity, E_{SMA} (GPa)	–	62.5	39.7
	f_y as in Fig. 1(b) (MPa)	–	401	379
	f_{P1} as in Fig. 1(b) (MPa)	–	510	405
	f_{T1} as in Fig. 1(b) (MPa)	–	370	180
	f_{T2} as in Fig. 1(b) (MPa)	–	130	100
	ε_l as in Fig. 1(b) (%)	–	6.00	5.5

Table 2
Calculation of plastic hinge lengths using different methods

Specimen	Cross-sectional area (mm^2)	d_b (mm)	L (mm)	f_y (MPa)	f_c' (MPa)	Experimental					Analytical			Empirical			
						Δ_y (mm)	Δ_u (mm)	ϕ_y (rad/km)	ϕ_u (rad/km)	L_p (Eq. (7)) (mm)	ϕ_y (rad/km)	ϕ_u (rad/km)	L_p (Eq. (5)) (mm)	L_p (Eq. (8)) (mm)	L_p (Eq. (9)) (mm)	L_p (Eq. (10)) (mm)	L_p (Eq. (11)) (mm)
Steel RC BCJ, JBC-1	100 000	19.5	1630	520	53.5	12	72	8.3	117	384	7.5	76.4	156	222	282	281	353
SMA RC BCJ, JBC-2	100 000	20.6	1630	401	53.7	18	72	22	122	374	18.0	91.3	131	222	282	281	312
SMA RC Column, SMAC-1 (Wang 2004)	72 966	12.7	1372	379	40.3	11	66	17	210	228	22.1	242.8	172	179	232	221	216

Table 3
Predicted maximum crack width and average crack spacing of specimen JBC-1 and JBC-2

Reference	Equation No.		Steel RC BCJ, JBC-1		SMA RC BCJ, JBC-2	
	w_{max} (mm)	S_m (mm)	w_{max} (mm)	S_m (mm)	w_{max} (mm)	S_m (mm)
Experimental	–	–	2.6	113.3	10.7	197.5
Oh and Kang [34]	Eq. (12)	Eq. (13)	5.1	130.7	6.7	133.3
CEB-FIP Code [35]	Eq. (16)	Eq. (14)	6.6	147.3	8.5	204.8
Chowdhury and Loo [39]	Eq. (20)	Eq. (18)	5.5	235.6	6.6	221.1
Eurocode 2 [40]	1.7 × Eq. (22)	Eq. (21)	2.9	141.1	10.0	223.1
Gergely–Lutz [37]	Eq. (17)	–	0.48	–	0.46	–
Masmoudi et al. [38]	Eq. (17)	–	1.8	–	1.7	–

steel and SMA-RC beam–column elements and compares findings with the experimental results. The bond-slip relationship and joint shear have also been discussed.

5.1. Moment–curvature relationship

The flexural behaviour of a RC section largely depends on the relationship between moment, curvature, and axial force. The moment (M)–curvature (φ) relationship depends on the material properties, geometry and arrangement of rebars in the cross-section of a RC member.

It is important to make proper assumptions for stress (σ)–strain (ε) curves of the materials for accurate prediction of the M–φ relationship. Scott et al. [29] model has been used for the σ–ε relationship of confined concrete, while the bilinear kinematic strain hardening model has been used for steel and SMA σ–ε curves with strain hardening parameters of 0.020 and 0.037, respectively. At large strains, unconfined concrete, outside the stirrups will spall off and will not contribute to the capacity of the member. Since this spalling is usually a gradual process, it is difficult to determine a particular strain at which spalling commences. It is assumed that the cover concrete follows the σ–ε curve of unconfined concrete according to the Scott et al. [29] model up to a strain of 0.004, but carries no stresses at higher strains. An incremental deformation technique has been used to determine the moment and its corresponding curvature at a particular strain distribution.

Fig. 5 shows the theoretical M–φ diagrams for the beams of JBC-1, JBC-2 and SMAC-1. The cracking moment of JBC-1 was 22.7 kN m at a curvature of 0.42 rad/km, whereas JBC-2 experienced cracking at a moment of 19.1 kN m at a curvature of 0.43 rad/km. The yield moments were reached at curvatures of 7.5 rad/km and 18.0 rad/km for JBC-1 and JBC-2, respectively. However, the moment capacities of JBC-1 and JBC-2 were found to be almost equal. The energy dissipation capacities of JBC-1 and JBC-2 under static loading were calculated as 1.1 kN m and 0.87 kN m, respectively using M–φ diagrams. It was observed that specimen JBC-2 and SMAC-1 suffered a significant amount of curvature before yielding of SMA compared to that of JBC-1. This is mainly due to the lower stiffness of SMA rebar compared to that of steel. SMAC-1 showed larger ductility compared to JBC-1 and JBC-2, which is mainly due to higher confinement by spiral reinforcements.

5.2. Plastic hinge length

The plastic hinge length of a structural member is an essential parameter in evaluating the response of a structure and its damage

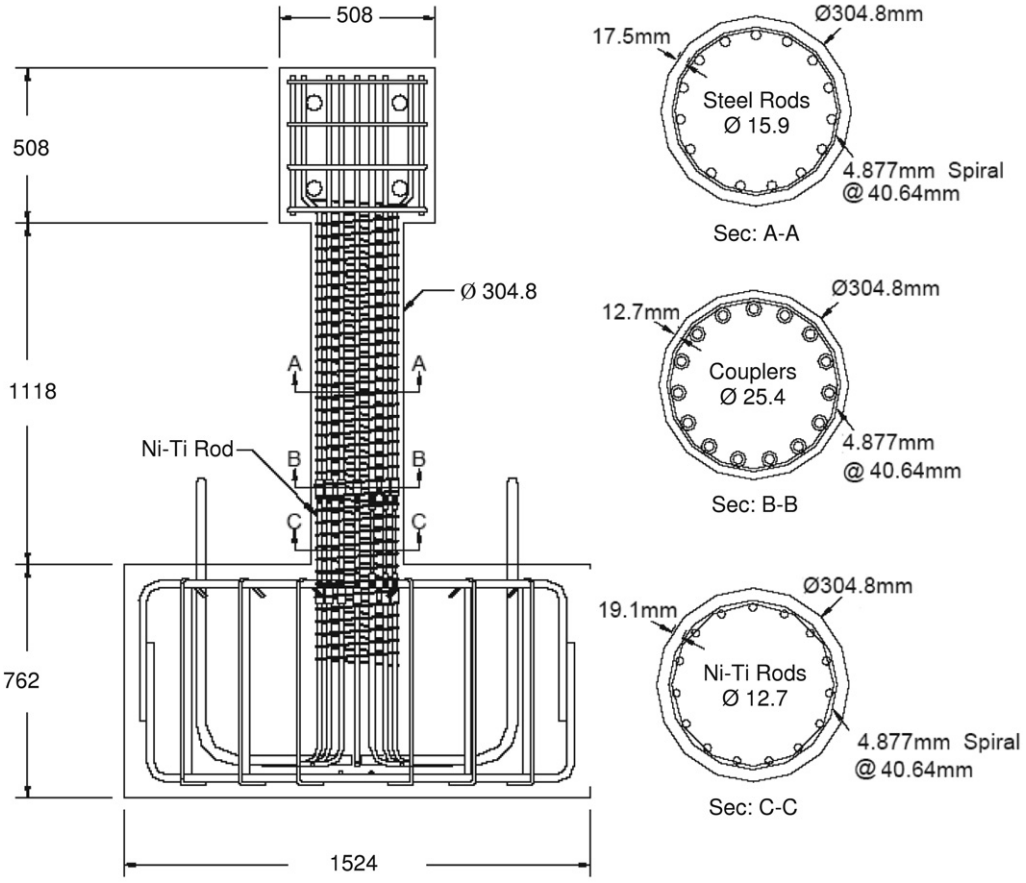

Fig. 4. Reinforcement details of SMA RC Column (Saiidi and Wang [14], with permission).

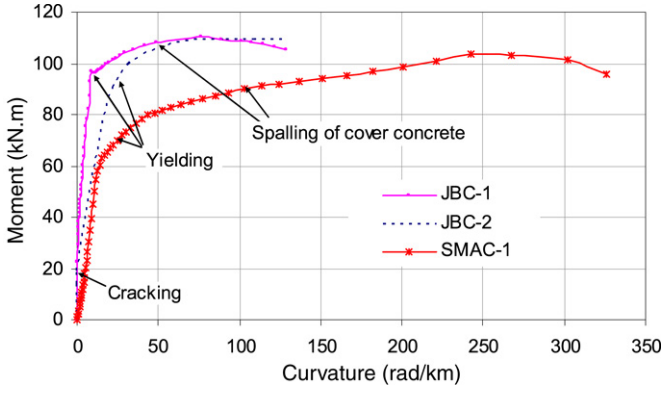

Fig. 5. Moment–curvature relationship of JBC-1, JBC-2, and SMAC-1.

due to seismic and/or other loads. Numerous techniques and models are available to estimate the plastic hinge length of RC members as described below.

5.2.1. Analytical method

From the moment–curvature relationship of a RC section, the ultimate moment can be chosen. Its corresponding load is calculated and applied at the beam/column tip. Subsequently, the curvature is distributed along the member length with respect to its moment ordinates. The curvature distribution along the length of the member (L) is constructed for specimens JBC-1, JBC-2 and SMAC-1 (Fig. 6) in order to determine their plastic hinge rotation and length. The rotation of the beam from the beam tip and column face, θ can be calculated by summing the curvature over its entire length, which is the summation of elastic rotation (θ_e) and plastic rotation (θ_p) (Eq. (1)). The curvature distribution is then idealized with distinct yield and ultimate curvature values. To create this model, a line, OE is extended from the origin parallel to the initial part of the curvature-distance graph as shown in Fig. 6. A perpendicular line, AB is drawn from the point of maximum curvature ordinate, A to the distance axis where AB intersects OE at E. Here, E and A represent the yield and ultimate curvature points. Line CD is drawn parallel to AB such that the sum of the areas of the parallelogram ACDE and triangle OBE equals the area under the curvature-distance curve, where DE or AC represents the plastic hinge length of the member [1]. Then the elastic and plastic rotation can be defined according to Eqs. (2) and (3), from which θ_p and L_p can be evaluated as shown in Eqs. (4) and (5), respectively. Here, ϕ_y represents the curvature at which, the rebar reaches its yield value, and ϕ_u represents the maximum curvature in the inelastic range.

$$\theta = \int_L \varphi.\mathrm{d}x = \theta_e + \theta_p \tag{1}$$

$$\theta_e = \phi_y \frac{L}{2} \tag{2}$$

$$\theta_p = \left(\phi_u - \phi_y\right) L_p \tag{3}$$

$$\theta_p = \theta - \theta_e \tag{4}$$

$$L_p = \frac{\int_L \phi.\mathrm{d}x - \phi_y \frac{L}{2}}{\phi_u - \phi_y}. \tag{5}$$

5.2.2. Experimental method

Beam tip displacement test data from reversed cyclic loading of beam–column joint specimens have been used to determine

Fig. 6. Curvature distribution along the member length of specimen (a) JBC-1, (b) JBC-2, and (c) SMAC-1.

the real plastic hinge lengths [1]. From force–displacement and moment–curvature test results, bilinear elastic perfectly plastic models have been used to obtain the yield and ultimate values of ϕ_y, ϕ_u, Δ_y and Δ_u. In order to determine the equivalent bilinear curve for the test results, the area under the curve (force–displacement or moment–curvature) is calculated, and then a line having the initial slope of the curve is drawn through the origin. A horizontal line is drawn such that the area under the two lines is equal to the area under the original curve. Then the yield displacement/curvature is defined as the point of intersection between the two lines and the ultimate value is considered as the maximum value of the displacement/curvature in the inelastic range. The Eqs. (6) and (7) can be solved to determine the value of L_p.

$$\Delta_p = \Delta_u - \Delta_y \tag{6}$$

$$\Delta_p = \left(\phi_u - \phi_y\right) L_p \left(L - \frac{L_p}{2}\right) \tag{7}$$

where, Δ_y and Δ_u represent the yield and ultimate beam tip displacement from test data, respectively.

5.2.3. Empirical methods

Empirical equations can also be used to estimate L_p for RC members. Numerous models are available. Many of these models consider a proportional increase of L_p with an increase of member length, depth and longitudinal reinforcement dimensions. For instance, models proposed for estimating L_p by Sawyer [30], Corley [31], Mattock [32], and Paulay and Priestley [33] are presented in Eqs. (8)–(11), respectively.

$$\text{Sawyer [30]: } L_p = 0.075L + 0.25d \tag{8}$$

$$\text{Corley [31]: } L_p = 0.5d + L/\sqrt{d} \tag{9}$$

$$\text{Mattock [32]: } L_p = 0.05L + 0.5d_b \tag{10}$$

$$\text{Paulay and Priestley [33]: } L_p = 0.08L + 0.022d_b f_y \tag{11}$$

where d represents the effective depth of the member in mm, d_b represents the bar diameter in mm, and f_y is the yield strength of the rebar in MPa.

The applicability of these methods for determining L_p of SMA RC members has been investigated and presented in Table 2. The results indicate that the analytical predictions from Eq. (5) provided much lower values compared to those of the experimental results. All the empirical equations underestimated the L_p values for beam–column joints. In the case of SMA-RC column, the estimations from all empirical equations were very close to the experimental value, except for Eq. (8). Eqs. (9) and (10) produced values relatively closer to the experimental results for all three specimens. The best prediction was obtained from Eq. (11), which could estimate the plastic hinge lengths of conventional steel RC members as well as SMA RC members with reasonable accuracy.

5.3. Crack width and crack spacing

Cracking of concrete significantly influences the structural performance of RC members including its stiffness and strength, ductility, energy absorption capacity, corrosion resistance and overall aesthetic appearance. Therefore, it is very important for designers to predict the crack width accurately. This section examines related models available in the literature and compares their results with experimental values for predicting the maximum crack width and average crack spacing of steel RC members and SMA RC members.

Oh and Kang [34] found that steel strain (ε_s), which is directly related to the applied loading, is the most important parameter that affects crack width. Other important variables affecting the crack width include the bar diameter (d_b), concrete clear cover (C), and effective tensile area of concrete (A_{ceff}) based on the energy concept. Oh and Kang [34] proposed the following formulas for predicting the maximum crack width, $w_{\max}$ and crack spacing, S_m.

$$w_{\max} = a_0 d_b \left(\varepsilon_s - 0.002\right) \frac{h_2}{h_1} \tag{12}$$

$$S_m = d_b \left[25.7 \left(\frac{C + d_b/2}{h_2}\right)^{4.5} + 1.66 \left(\frac{A_{\text{ceff}}/n}{A_{s1}}\right)^{1/3} + \frac{0.236 \times 10^{-6}}{\varepsilon_s^2}\right] \tag{13}$$

in which, $a_0 = 159 \left(\frac{C+d_b/2}{h_2}\right)^{4.5} + 2.83 \left(\frac{A_{\text{ceff}}/n}{A_{s1}}\right)^{1/3}$, h_1 = distance from the centroid of the tension rebar to the neutral axis (mm), h_2 = distance from the extreme tension fiber to the neutral axis (mm), n = number of rebar in the tension zone, and A_{s1} = area of each rebar.